

**Part 1: Temporal
variability**

H. Mao and R. Talbot

This discussion paper is/has been under review for the journal Atmospheric Chemistry and Physics (ACP). Please refer to the corresponding final paper in ACP if available.

Speciated mercury at marine, coastal, and inland sites in New England – Part 1: Temporal variability

H. Mao¹ and R. Talbot²

¹Department of Chemistry, State University of New York, College of Environmental Science and Technology, Syracuse, NY 13219, USA

²Department of Earth and Atmospheric Sciences, University of Houston, Houston, TX 77204, USA

Received: 27 September 2011 – Accepted: 16 November 2011
– Published: 8 December 2011

Correspondence to: H. Mao (hmao@esf.edu)

Published by Copernicus Publications on behalf of the European Geosciences Union.

Title Page

Abstract

Introduction

Conclusions

References

Tables

Figures

◀

▶

◀

▶

Back

Close

Full Screen / Esc

Printer-friendly Version

Interactive Discussion



Abstract

A comprehensive analysis was conducted using long-term continuous measurements of gaseous elemental mercury (Hg^0), reactive mercury (RGM), and particulate phase mercury (Hg^P) at coastal (Thompson Farm, denoted as TF), marine (Appledore Island, denoted as AI), and elevated inland (Pac Monadnock, denoted as PM) sites from the AIRMAP Observatories. Decreasing trends in background Hg^0 were identified in the 7- and 5-yr records at TF and PM with decline rates of 3.3 parts per quadrillion by volume (ppqv yr^{-1} and 6.3 ppqv yr^{-1} , respectively). Common characteristics at these sites were the reproducible annual cycle of Hg^0 with its maximum in winter-spring and minimum in fall as well as a decline/increase trend in the warm/cool season. The coastal site TF differed from the other two sites with its exceptionally low levels (as low as below 50 ppqv) in the nocturnal inversion layer probably due to dissolution in dew water. Year-to-year variability was observed in the warm season decline in Hg^0 at TF varying from a minimum total seasonal loss of 20 ppqv in 2010 to a maximum of 92 ppqv in 2005, whereas variability remained small at AI and PM. Measurements of Hg^0 at PM, an elevated inland rural site, exhibited the smallest diurnal to annual variability among the three environments, where peak levels rarely exceeded 250 ppqv and the minimum was typically 100 ppqv. It should be noted that summertime diurnal patterns at TF and AI are opposite in phase indicating strong sink(s) for Hg^0 during the day in the marine boundary layer, which is consistent with the hypothesis of Hg^0 oxidation by halogen radicals there. Mixing ratios of RGM in the coastal and marine boundary layers reached annual maximum in spring and minimum in fall, whereas at PM levels were generally below the limit of detection (LOD) except in spring. RGM levels at AI were higher than at TF and PM indicating a stronger source strength(s) in the marine environment. Mixing ratios of Hg^P at AI and TF were close in magnitude to RGM levels and were mostly below 1 ppqv. Diurnal variation in Hg^P was barely discernible at TF and AI in spring and summer with higher levels during the day and smaller but above the LOD at night.

Part 1: Temporal variability

H. Mao and R. Talbot

Title Page

Abstract

Introduction

Conclusions

References

Tables

Figures

◀

▶

◀

▶

Back

Close

Full Screen / Esc

Printer-friendly Version

Interactive Discussion



1 Introduction

Atmospheric mercury exists in three forms, gaseous elemental mercury (Hg^0), reactive gaseous species ($\text{RGM} = \text{HgCl}_2 + \text{HgBr}_2 + \text{HgOBr} + \dots$), and particulate mercury (Hg^P). Hg^0 can be oxidized to RGM, part of which is further transformed to Hg^P on aerosol surfaces. RGM and Hg^P eventually enter the biosphere via dry and wet deposition. Hg^0 reportedly has a lifetime of 6-12 months, whereas RGM and Hg^P are highly soluble and thus quickly removed from the atmosphere (Schroeder and Munthe, 1998). In general Hg^0 comprises >95 % of total gaseous mercury ($\text{TGM} = \text{Hg}^0 + \text{RGM}$). However, studies suggest that fractions of Hg^0 , RGM, and Hg^P of total atmospheric mercury vary geographically due to different land surface types, chemical environments, and human influences.

There have been world-wide measurements of ambient levels of Hg^0 and TGM. A recent review by Sprovieri et al. (2010, references therein) summarized that the background level of atmospheric total gaseous mercury (TGM) in the Northern Hemisphere ranges from 1.5 to 1.7 ng m^{-3} (i.e. 168–190 ppqv based on $1 \text{ ng m}^{-3} = 112 \text{ ppqv}$ in a standard atmosphere). For rural and mountainous sites in the northeastern and southeastern US, Sigler and Lee (2006) and Valente et al. (2007) suggested typical levels of Hg^0 at $\sim 1.6 \text{ ng m}^{-3}$. Our previous study found a regional background level of $\sim 160 \text{ ppqv}$ (i.e. 1.4 ng m^{-3}) in wintertime New England (Mao et al., 2008). In the marine environment, Hg^0 is reportedly around 1.6 ng m^{-3} over the North Atlantic (Laurier and Mason, 2007), $1.6\text{--}4.7 \text{ ng m}^{-3}$ over the North Pacific (Laurier et al., 2003), and $0.4\text{--}11.2 \text{ ng m}^{-3}$ over the Mediterranean Sea (Sprovieri et al., 2003).

In comparison, there is much less coverage of RGM and Hg^P measurements in space and time. The review by Valente et al. (2007; references therein) suggested mean RGM and Hg^P concentrations over land to be 0.029–0.048 and 0.029–0.361 ng m^{-3} respectively. Mason et al. (2003, references therein) compiled available oceanic measurements of RGM and Hg^P and reported a wide range of average

Part 1: Temporal variability

H. Mao and R. Talbot

Title Page

Abstract

Introduction

Conclusions

References

Tables

Figures

◀

▶

◀

▶

Back

Close

Full Screen / Esc

Printer-friendly Version

Interactive Discussion



Part 1: Temporal variability

H. Mao and R. Talbot

Title Page

Abstract

Introduction

Conclusions

References

Tables

Figures

◀

▶

◀

▶

Back

Close

Full Screen / Esc

Printer-friendly Version

Interactive Discussion



concentrations. In the marine atmosphere RGM varied from 6 (± 6) pg m^{-3} north of 30° N over the Pacific (Laurier et al., 2003) to a high of 50 (± 43) pg m^{-3} at Bermuda downwind of North America (Sheu, 2001). Over the North Atlantic Laurier and Mason (2007) found a value of 5.9 pg m^{-3} for RGM concentrations averaged over a 10 day period in late summer with maximum values reaching 27 pg m^{-3} . A level of 8 $\text{pg Hg}^{\text{P}} \text{m}^{-3}$ was measured at Mace Head, Ireland (Ebinghaus et al., 2002), compared to much higher values of 31 (± 44) pg m^{-3} in coastal Maryland (Mason and Sheu, 2002). The four two-week measurement campaigns during the MAMCS project in the Mediterranean region over the 1998–2000 period showed that RGM concentrations in the Mediterranean, far from sources and particularly with onshore winds, were comparable to those in industrial northern Europe (Pirrone et al., 2003).

In the northeastern US, we showed an annual mean RGM mixing ratio of 0.41 (± 0.93) ppqv with a range of 0–22 ppqv at a rural site on the southern New Hampshire coastline in 2007 compared to the annual mean of 0.13 (± 0.25) ppqv and a median below the limit of detection (LOD) (0.1 ppqv) at an elevated (700 m altitude) 185 km inland site) (Sigler et al., 2009). In the same study we found mean RGM at a marine site during July–September 2007 to be 0.76 (± 0.88) ppqv, significantly higher than those at coastal and inland sites for the same time period.

In a recent study on the long-term trend in background Hg^{O} , Ebinghaus et al. (2011) reported a decline rate of $-0.028 \pm 0.01 \text{ ng m}^{-3} \text{ yr}^{-1}$ (equivalent to $3.1 \pm 1.1 \text{ ppqv yr}^{-1}$) based on monthly mean values of baseline data for the 1996–2009 period at Mace Head, Ireland. A decline of $-0.034 \pm 0.005 \text{ ng m}^{-3} \text{ yr}^{-1}$ (equivalent to $3.8 \pm 0.6 \text{ ppqv yr}^{-1}$) was found from background data at Cape Point in South Africa by Slemr et al. (2011). At Alert Cole and Steffen (2010) found a 0.6% yr^{-1} decreasing rate in Hg^{O} over the time period of 1995–2007. This study presented the first opportunity to look into possible trends in background Hg^{O} at midlatitudes in the Northeastern US.

Multiple-year detailed and continuous measurements of Hg^{O} , RGM, and Hg^{P} have been conducted at inland, coastal, and marine locations from the AIRMAP

Observatory. In this study, we aimed to obtain a comprehensive analysis of Hg^0 , RGM, and Hg^{P} variations ranging from diurnal to interannual time scales at locations with distinct geographic and environmental characteristics.

2 Measurements and approach

5 Observations of Hg^0 , RGM, and Hg^{P} were conducted at three AIRMAP (www.airmap.unh.edu) Observatory sites: Thompson Farm (43.11° N, 70.95° W, 24 m a.g.l.) (TF), Pac Monadnock (42.86° N, 71.88° W, 700 m a.g.l.) (PM), and Appledore Island (42.97° N, 70.62° W, 40 m a.g.l.) (AI) (Fig. 1). The PM and TF sites are 185 and 25 km, respectively, inland from the Atlantic Ocean, while AI is 10 km offshore in the Gulf of
10 Maine. The locations of the three sites form a unique west-east oriented transect with site surroundings composed of heavily forested, coastal, and marine boundary layer environments. Moreover, due to the remote central location of PM in New England and its 700 m elevation (i.e. above the nocturnal inversion and in the middle of the daytime boundary layer), the site is ideally located to determine regional trends in trace gases, including mercury (Mao and Talbot, 2004; Mao et al., 2008).

Mercury instruments were operated in a manner identical at TF, PM, and AI to ensure data consistency. Continuous Hg^0 measurements with 5-min resolution have been ongoing since November 2003 at TF, June 2005 at PM, and June 2007 on AI. Measurements of RGM with 2-h resolution were added in November 2006 at TF, December 2006
20 at PM, and June 2007 on AI. Measurements of Hg^{P} started at TF in February 2009 and on AI in April 2009. The end date for the study period in this paper for Hg^0 , RGM, and Hg^{P} is 31 August 2010, except that at PM the RGM measurement was terminated in October 2008.

25 A Tekran 1130 denuder module operated in series with the 2537A provided continuous measurements of both RGM and Hg^0 respectively. A custom cold finger trap was used to remove water vapor before the air stream enters the pump module, which has been used at TF and PM for over 2 yr (Sigler et al., 2009). Ambient mixing ratios

Part 1: Temporal variability

H. Mao and R. Talbot

Title Page

Abstract

Introduction

Conclusions

References

Tables

Figures

◀

▶

◀

▶

Back

Close

Full Screen / Esc

Printer-friendly Version

Interactive Discussion



of Hg⁰ were measured continuously using the 2537A cold vapor atomic fluorescence spectrometer with 5-min time resolution and a LOD of ~10 ppqv (1 ng m⁻³ = 112 ppqv). Details of operation of the 2537A can be found in Mao et al. (2008).

RGM is measured with a 90 min sampling interval yielding a LOD of ~0.1 ppqv based on three times the standard deviation of the field blank values determined at TF during 2007. To ensure clean operation, the KCl-coated denuders, denuder module glassware, impactor frits and sample filters (all prepared in a clean room) are replaced on a bi-weekly basis. Zero air cartridges and soda lime traps were replaced as needed. Clean operation was verified by flushing of zero air (Hg-free) through the 1130 denuder module into the 2537A. No direct calibration method has been developed for the Tekran 1130 speciation unit, although thermal desorption and reduction of RGM to Hg⁰, with subsequent analysis by the 2537A, is reported to be essentially 100 % efficient (Landis et al., 2002; Sigler et al., 2009).

The inlet of the 1135 Hg^P Tekran at AI had an elutriator inlet with an acceleration jet to remove aerosols >2.5 μm so that only fine Hg^P is measured. This is not a desirable design, especially in the marine environment with sea salt in the 2–10 μm range. Since our goal was to elucidate mercury cycling, the total amount of mercury in the aerosol phase must be determined accurately. We replaced the elutriator with one that contained no impaction plate to facilitate collection of coarse aerosols on the quartz frit in the Tekran 1135 (Talbot et al., 2011). This produced satisfactory results on average when compared to bulk collection on a Teflon filter, except when Hg^P values were above 1 ppqv (Talbot et al., 2011). In these cases the Tekran underestimated Hg^P by as much as a factor of 3.

Measurement data of carbon monoxide (CO) were used in this study in determining anthropogenic influence. A description of CO measurement can be found in Mao and Talbot (2004).

Part 1: Temporal variability

H. Mao and R. Talbot

Title Page

Abstract

Introduction

Conclusions

References

Tables

Figures

◀

▶

◀

▶

Back

Close

Full Screen / Esc

Printer-friendly Version

Interactive Discussion



3 Hg⁰, RGM, and Hg^P at marine, coastal and inland sites

3.1 Seasonal and annual variations

The complete time series of 5-min average Hg⁰ mixing ratios for the time periods of availability at AI, TF, and PM are displayed in Fig. 2. The nearly 7, 5, and 3 yr datasets at TF, PM, and AI, respectively, reproduced the annual cycle with an annual maximum in late winter–early spring and a minimum in early fall as identified in Mao et al. (2008). In the extended dataset presented in this study, TF consistently exhibited precipitous day-to-day dips and peaks that reached as low as ~50 ppqv in early fall compared to the highest levels exceeding 300 ppqv in late winter–early spring. Trends at AI tracked those at TF well, although the diurnal minimum did not plunge to the low levels at TF and the diurnal maximum often exceeded that at TF. In comparison, Hg⁰ at the elevated rural inland site PM revealed much smaller diurnal-to-annual variations and much higher minimum values. At PM daily maximum mixing ratio rarely exceeded 250 ppqv with the minimum typically ~100 ppqv, consistent with Mao et al. (2008).

One distinct feature that set TF apart from AI and PM was the lowest levels of Hg⁰ (<50 ppqv) occurred in summer and fall, which appears to be due to dry deposition of Hg⁰ under the nocturnal inversion layer (Mao et al., 2008). A comparison of Hg⁰ seasonal statistics at the three sites is summarized in Table 1. The difference in the 10th percentile, median and 90th percentile values of Hg⁰ between the three sites does not reveal distinct patterns over the years. One exception was that the lowest 10th percentile values at TF in summer and fall were lower than PM by 11–44 ppqv over the period from 2004 to 2010. The 10th percentile values at AI were ~110 ppqv for the three summers (2007–2010), lower than PM by 10–20 ppqv. Winter and spring median values from TF appeared to be close to those at PM with an exception of being 20–30 ppqv higher in 2009. Note that values at AI in the 2009 winter and spring were close to those at PM. This may imply localized sources of Hg⁰ at TF during the 2009 winter and fall.

Part 1: Temporal variability

H. Mao and R. Talbot

Title Page

Abstract

Introduction

Conclusions

References

Tables

Figures

◀

▶

◀

▶

Back

Close

Full Screen / Esc

Printer-friendly Version

Interactive Discussion



Part 1: Temporal variability

H. Mao and R. Talbot

[Title Page](#)[Abstract](#)[Introduction](#)[Conclusions](#)[References](#)[Tables](#)[Figures](#)[◀](#)[▶](#)[◀](#)[▶](#)[Back](#)[Close](#)[Full Screen / Esc](#)[Printer-friendly Version](#)[Interactive Discussion](#)

The decline and increase rates of Hg^0 in the warm and cool seasons, respectively, were calculated and examined for the three sites (Table 2). The warm season spans the time period between the times of the annual maximum and minimum, approximately 1 April to 30 September at TF, 1 March to 31 October at AI, and 1 March to 31 October at PM. The cool season extends from the time of the annual minimum to that of the following annual maximum. A few main characteristics can be summarized as follows.

First, at all three sites, there was much less year-to-year variability in the cool season increase rate at all three sites. Increase rates were ~ 0.3 ppqv day^{-1} at AI, 0.4 – 0.5 ppqv day^{-1} at TF, and ~ 0.3 ppqv day^{-1} at PM except the falls of 2005 (0.1 ppqv day^{-1}) and 2009 (0.5 ppqv day^{-1} with data in November missing). Total seasonal increases were ~ 50 ppqv at AI, 52 – 69 ppqv at TF, and ~ 40 ppqv at PM (except ~ 20 ppqv in fall 2005). Mixing ratios of Hg^0 in the marine and coastal environments increased more than at a rural elevated location during the cool season. This indicates that as the cool season started in late September and early October Hg^0 , sinks may be reduced and/or sources enhanced in the marine and coastal environments more strongly than at a remote site like PM. During that time of the year enhanced sources are likely associated with coal and natural gas combustion as well as wood burning for residential heating in the region. Weakened sinks could be linked to plant senescence, which reduces the surface area for Hg^0 uptake, as well as snow cover for which dry deposition velocities of Hg^0 are two to four orders of magnitude smaller than for other surface types (Zhang et al., 2009, and references therein). The slower increasing rate at PM might reflect its relatively remote location and higher altitude where anthropogenic influence is dampened compared to AI and TF that are closer to source regions.

Second, the decline rate of Hg^0 during warm seasons at TF varied greatly from year to year compared to relatively small ranges at AI and PM with some exceptions. The maximum warm season decline rate 0.6 ppqv day^{-1} occurred at TF in 2005 yielding a total seasonal loss of 92 ppqv and the minimum 0.1 ppqv day^{-1} resulting a total decrease of 22 ppqv in 2010. This suggests that at TF there were unique processes

Part 1: Temporal variability

H. Mao and R. Talbot

Title Page

Abstract

Introduction

Conclusions

References

Tables

Figures

◀

▶

◀

▶

Back

Close

Full Screen / Esc

Printer-friendly Version

Interactive Discussion



that set its warm season decline rates apart from the other two environments. Mao et al. (2008) identified two warm seasons in 2004 and 2005 with drastically different decline rates of Hg^0 at TF and speculated that the large difference in precipitation from 2004 to 2005 observed at the site may have been the main cause. At the time there were barely two years of data at PM over 2005–2007 which could not be compared with the two contrasting seasons at TF. In this study as the 5-yr dataset at PM from 2005 to 2010 was examined, unlike TF, the 2005 warm season decline rate at PM did not appear to stand out as an anomaly. Our previous studies demonstrated that measurements at PM are representative of regional air pollution (Mao and Talbot, 2004; Mao et al., 2008), and therefore the peak decline rate at TF during the 2005 warm season appeared to be a localized phenomenon instead of a regional one. Indeed, the reports from the Northeastern Regional Climate Center (<http://www.nrcc.cornell.edu/>) suggested that the 2005 spring in New Hampshire was a normal spring and the summer was warmer and wetter, but not to the extreme, regarding temperature and precipitation in the context of a 116 yr climate record. Summers 2006, 2008, and 2009 were among the wettest on the record, and yet the warm season decline rates during those three years were average. In-depth study is warranted to understand and identify the mechanism(s) driving the decline/increasing patterns as well as the year-to-year variability in such patterns.

The overall trends in background Hg^0 at the three sites were examined in Fig. 3. We parsed out data with CO below its 25th percentile value to represent the background atmosphere and calculated monthly median mixing ratios of background Hg^0 . There appeared to be decreasing trends in background Hg^0 at TF and PM with decline rates of 3.3 ppqv yr^{-1} and 6.3 ppqv yr^{-1} , respectively. The trend at AI was inconclusive because of a limited number of years of measurements. This suggests that in an elevated rural environment, which is above the boundary layer half of the time (i.e. at night), background Hg^0 mixing ratios were decreasing at a pace nearly a factor of 2 faster than that in a northeastern US coastal environment, although the time period of the TF dataset was 1.3 yr longer than the PM one. The decline rate at TF was comparable

to the ones from Mace Head, Ireland (Ebinghaus et al., 2011) and Cape Point, South Africa (Slemr et al., 2011), while caution should be taken in such comparison as the time periods in Ebinghaus et al. (2011) and Slemr et al. (2011) were nearly twice as long as ours. We will investigate the possible factors that might have contributed to these trends in a separate paper (Mao and Talbot, 2011).

The complete time series of RGM at the three sites exhibited distinct annual cycles in the upper range of mixing ratios (Fig. 4). Specifically, the annual cycle in the 90th percentile RGM levels at AI and TF displayed maxima in spring and minima in fall, while at the inland site PM, values in all seasons were below the LOD (0.1 ppqv), except in springtime (Table 3). Three key points can be summarized regarding the 10th percentile, median, and 90th percentile values. First, a common characteristic in RGM at the marine, coastal, and inland sites is near-zero 10th percentile values. Second, RGM mixing ratios were generally lowest at PM, with median values and 90th percentile values hardly exceeding 0.5 ppqv throughout the 7 seasons, even though two coal-fired power plants are located nearby, Salem Harbor and Merrimack Stations 168 km south and 119 km north of PM, respectively. This is consistent with observations from other geographic locations, such as the site on the eastern slope of Mt. Gongga in China (Fu et al., 2008) with two industrial areas located 50–60 km south and southeast of the sampling site, where RGM is lost relatively fast via dry deposition after leaving its sources. Third, larger median and 90th percentile mixing ratios were observed in the marine environment than at the coastal and inland locations in all seasons except the winter, spring and summer of 2009 when RGM mixing ratios at TF were uncharacteristically higher. The last point indicates stronger source strength(s) for RGM in the marine environment, which alludes to the possibility of more Hg^0 oxidized by abundant halogen radicals there leading to higher RGM mixing ratios.

Mixing ratios of Hg^{P} at AI and TF were close in magnitude to RGM levels and were mostly below 1 ppqv except the samples above the 90th percentile values in February 2009 and the ensuing spring at TF (Fig. 5 and Table 4). Observations at TF revealed that the annual maxima occurred in winter and minima in fall, which is similar to the

Part 1: Temporal variability

H. Mao and R. Talbot

[Title Page](#)[Abstract](#)[Introduction](#)[Conclusions](#)[References](#)[Tables](#)[Figures](#)[◀](#)[▶](#)[◀](#)[▶](#)[Back](#)[Close](#)[Full Screen / Esc](#)[Printer-friendly Version](#)[Interactive Discussion](#)

annual cycle of RGM. This appears to be reasonable because maximum RGM in later winter/early spring makes it possible for maximum conversion of RGM to Hg^{P} via deposition to aerosol surfaces.

3.2 Diurnal variation

Hg^{O} : seasonally averaged diurnal cycles are shown in Figs. 6–8 for all years at the three sites. Our previous study (Mao et al., 2008) using 3- and 2-yr Hg^{O} measurements data at TF and PM revealed that the largest diurnal variability occurred in the fall at TF with a seasonal averaged daily amplitude of ~ 20 ppqv, whereas the diurnal variation at PM was flat year-round except in the 2006 summer with a seasonal averaged daily amplitude of ~ 10 ppqv. In this study the 7-yr dataset suggested that seasonality in Hg^{O} diurnal variation was reproduced unfailingly every year at the three sites with remarkable interannual variability in some seasons depending on site location (Figs. 6, 7, 8). At TF (Fig. 6), the diurnal variation was nearly flat in all 7 winters followed by increases to a daily amplitude of ~ 10 – 20 ppqv in spring and was most pronounced in summer and fall with a daily amplitude ranging from 20 to 40 ppqv. The daily minimum occurred before sunrise and reached maximum values at $\sim 14:00$ UTC in spring and $\sim 15:00$ UTC in summer and fall.

As suggested in Mao et al. (2008), nighttime low levels of Hg^{O} at TF in the warm season resulted from the occurrence of the nocturnal inversion at altitudes below ~ 300 m in New England. A box modeling study by Kim (2010) found that using the Henry's Law coefficient of 0.13 M atm^{-1} for Hg^{O} and initial conditions of 170 ppqv Hg^{O} , 25°C temperature, and liquid water content of $10^{-10} (\text{m}_{\text{water}}^{-3}/\text{m}_{\text{air}}^{-3})$, the atmospheric level of Hg^{O} decreased from 170 ppqv to zero after 30 h. On summer nights when a nocturnal inversion layer formed at our local field site, often the Hg^{O} mixing ratio was observed to decrease from 120 ppqv to 80 ppqv over 10 h on average reaching its minimum value just before sunrise. On those nights there was abundant dew formation due to radiative cooling at the surface; should the same amount of dew remain for 20 more hours and the Hg^{O} level continue to decrease at the same rate, the atmospheric Hg^{O} level

Part 1: Temporal variability

H. Mao and R. Talbot

Title Page

Abstract

Introduction

Conclusions

References

Tables

Figures

◀

▶

◀

▶

Back

Close

Full Screen / Esc

Printer-friendly Version

Interactive Discussion



could be reduced to zero. The fact that this estimate is close to box model results from Kim (2010) indicates that the observed nighttime depletion of Hg^0 is highly likely caused by Hg^0 dissolving into dew. This implies that the observed 40 ppqv Hg^0 dissolved in dew would largely be re-volatilized after sunrise if not all, and thus the increase in Hg^0 mixing ratios between sunrise and 15:00 UTC in summer can be ascribed chiefly to Hg^0 re-volatilization from dew alone.

From the three-year dataset at AI emerged one of the most interesting characteristics in the diurnal variation of Hg^0 in the summertime marine boundary layer (see summers in Fig. 7). It is opposite in phase to that at TF (see summers in Fig. 6), with daily maxima before sunrise and minima in the time window of 20:00–00:00 UTC. There appeared to be a net loss of Hg^0 around 10 ppqv during the day at AI (daily maximum-minimum). This was also documented in Sigler et al. (2009) where a 2-month dataset in July–September 2007 suggested opposite diurnal cycles of Hg^0 and RGM at AI. This pattern was reproduced in summers 2008, 2009 and 2010 with nearly identical patterns and magnitude. We speculated that the net loss of Hg^0 during the day was possibly caused by oxidation by abundant halogen radicals in the marine boundary layer (Sigler et al., 2009).

Compared to TF and AI, diurnal variation at PM appeared to be nearly flat in all seasons except summers 2006 and 2009 with a seasonally average daily amplitude of 10 ppqv (Fig. 8). The seasonal variation in diurnal mixing ratios was relatively small, constrained within 20 ppqv in all five years. This lack of diurnal, seasonal and annual variation was attributed to its 700 m a.g.l. elevation, well above the nighttime boundary layer and thus the site is removed from direct influence of chemical and physical processes near the surface (Mao et al., 2008). Moreover, the winter and spring level at PM is close to that at TF and AI, reflecting the regional representativeness of the site, whereas in summer and fall it tended to be 20–30 ppqv higher indicating additional sink(s) at TF and AI. Compared to TF and AI, the standard deviation of means at PM appeared to be much smaller, indicating that at this elevated inland rural site there were less disturbances on time scales <10 min that could bring about changes in ambient

Part 1: Temporal variability

H. Mao and R. Talbot

[Title Page](#)[Abstract](#)[Introduction](#)[Conclusions](#)[References](#)[Tables](#)[Figures](#)[◀](#)[▶](#)[◀](#)[▶](#)[Back](#)[Close](#)[Full Screen / Esc](#)[Printer-friendly Version](#)[Interactive Discussion](#)

levels of Hg^0 than in the coastal and marine environments.

Two interesting features were apparent in interannual variability of seasonal averaged diurnal cycles at the three sites. First, among the three sites, TF experienced the most significant interannual variability in winter, spring, and fall diurnal cycles compared to the least amount at AI and PM constrained within ~ 20 ppqv. Note that at AI Hg^0 levels in fall 2007 were nearly 30 ppqv lower than the other two years (Fig. 7) due to limited data availability during 1–16 September only reflecting the lowest level of Hg^0 in a year. Second, both TF and AI exhibited the least interannual variability in summer compared to other seasons, whereas PM saw the reversed seasonal dependence of interannual variability. This raises the question whether such site differences reflect the marine-land or altitude difference, which can entail profound implications. Interannual variability in Hg^0 can result from influences of anthropogenic emissions, physical processes (i.e. driven by climate conditions), and chemistry. Hence, the site difference may suggest that at elevated inland rural locations interannual variability in ambient levels of Hg^0 is largely driven by processes in summer, whereas in the coastal and marine environments downwind of major source regions the net effect of all processes can vary greatly from year to year in all seasons except summer.

RGM: seasonal averaged diurnal cycles of RGM at TF, AI, and PM are illustrated in Figs. 9–11. There was distinct diurnal variation at TF and AI with maxima at 18:00–20:00 UTC and minima at 09:00–11:00 UTC, whereas it was almost flat at PM and near the LOD in all seasons except spring and winter 2007. The strongest diurnal variation occurred in springs 2007, 2008, and 2009 at TF, with daily amplitude exceeding 1 ppqv compared to 0.2–0.3 ppqv in other seasons. The highest seasonal average diurnal maxima also occurred in the same seasons reaching up to 1.7 ppqv, while daily maxima varied between the LOD and 0.7 ppqv in all other seasons. Nighttime mixing ratios were close to the LOD in summer and fall but were well above it in winters and springs of 2007–2009. Spring and winter 2010 at TF were exceptions with RGM mixing ratios mostly near the LOD.

Part 1: Temporal variability

H. Mao and R. Talbot

Title Page

Abstract

Introduction

Conclusions

References

Tables

Figures

◀

▶

◀

▶

Back

Close

Full Screen / Esc

Printer-friendly Version

Interactive Discussion



Part 1: Temporal variability

H. Mao and R. Talbot

[Title Page](#)[Abstract](#)[Introduction](#)[Conclusions](#)[References](#)[Tables](#)[Figures](#)[◀](#)[▶](#)[◀](#)[▶](#)[Back](#)[Close](#)[Full Screen / Esc](#)[Printer-friendly Version](#)[Interactive Discussion](#)

Similar patterns and magnitude were observed for the spring- and summertime diurnal variation at AI. Two unique features distinguished AI from TF. First, mixing ratios were close in range (0.2–1.5 ppqv) between all seasons except winter 2010. This implies that in the marine boundary layer there seemed to be net production of RGM in summer and spring as opposed to spring only in the coastal boundary layer. Second, more often than not nighttime mixing ratios remained above the LOD, typically over the range of 0.2–0.5 ppqv, except during fall 2009 which exhibited a higher range of 0.5–1.0 ppqv. In general, RGM production in the marine boundary layer is considered to be facilitated by halogen radical chemistry which is driven by solar radiation. Non-zero RGM at night indicates possible nighttime production mechanisms (e.g. involving NO_3), despite rapid removal by dry and wet deposition, in the marine environment in summer and spring.

Hg^{P} : seasonal averaged diurnal cycles of Hg^{P} at TF and AI are illustrated in Figs. 12 and 13. Generally, Hg^{P} mixing ratios were higher in winter–spring and lower in summer–fall at TF compared to little variation at AI in all seasons except winter 2010. For both sites one distinguishing feature is that compared to RGM, Hg^{P} mixing ratios showed significantly smaller daily amplitudes and smaller seasonal variability at a specific time of the day. At TF the seasonal averaged daily amplitude was 0.4 and 0.2 ppqv in winter and spring respectively, while it was negligible in summer and fall. It was ~ 0.2 ppqv at AI in spring, summer and fall. The 2010 wintertime diurnal cycle was uncharacteristically flat with mixing ratios remaining nearly constant at 0.1 ppqv.

The most prominent difference between the two sites lies in their diurnal patterns. At TF the daily maximum occurred at 17:00–20:00 UTC similar to RGM. However, at AI the pattern changed from season to season and from year to year, where the daily maximum occurred over 06:00–09:00 UTC in spring and summer 2009 compared to 17:00–20:00 UTC in fall 2009 and spring 2010. This large seasonal and year-to-year variability at AI indicates that the production and loss mechanisms controlling the ambient Hg^{P} level are more complex and multitudinous in the marine environment than in the coastal one.

Part 1: Temporal variability

H. Mao and R. Talbot

Title Page

Abstract

Introduction

Conclusions

References

Tables

Figures

◀

▶

◀

▶

Back

Close

Full Screen / Esc

Printer-friendly Version

Interactive Discussion



As aforementioned, RGM at AI was increased by 0.4 and 0.2 ppqv during the day in April and July, respectively, while Hg^{P} levels were quite constant throughout the day hovering around 0.1 ppqv in April and 0.3 ppqv in July. The RGM + Hg^{P} mixing ratios were less than 1 ppqv, which is $<1/10$ of the seasonal averaged daily loss of Hg^{O} . This implies that the majority of the RGM + Hg^{P} production during the summer is quite possibly lost through wet and dry deposition, if we assume that: (1) the lost amount of Hg^{O} was transformed to RGM + Hg^{P} , (2) the loss of Hg^{O} during the day was driven by oxidation while the total effect of deposition and oceanic emissions is similar in night- and daytime.

Lombard et al. (2011) calculated that the total wet deposition at TF in summer 2007 and 2008 were 3.02 and $6.37 \mu\text{g m}^{-2}$, which is approximately 338 and 750 ppqv using an average PBL height of 1000 m. In the same study they estimated a 2.31 cm s^{-1} dry deposition velocity of RGM in summer using an order-of-magnitude approach and three hourly mixing ratios of RGM and obtained a daily amount of dry deposition loss of RGM to be 92, 46, and 42 ppqv for summers 2007, 2008 and 2009. On a seasonal basis, the total loss of RGM from wet and dry deposition amounted to 430 and 796 ppqv in summers 2007 and 2008, which yields a daily average depositional loss of ~ 5 and ~ 9 ppqv. Assuming Hg^{P} levels and the dry deposition velocity of sea salt aerosols, on which most Hg^{P} resides (Feddersen et al., 2011), are similar to those of RGM, it may not be far-fetching to hypothesize that the amount of Hg^{P} lost via dry deposition is comparable to that of RGM. Thus in summer a daily loss of RGM and Hg^{P} via wet and dry deposition may be close to 10–20 ppqv, which explains why the lowest ambient mixing ratios of RGM + Hg^{P} occurred in summer.

4 Summary

In this study we present a comprehensive analysis of diurnal to seasonal variability in Hg^{O} , RGM, and Hg^{P} at an inland rural elevated site, a coastal site, and a marine site. The common characteristics at the three sites were similar seasonal median

mixing ratios of Hg^0 and the reproducible annual cycle of Hg^0 with maximum in winter-spring and minimum in fall, and the decline/increase in the warm/cool seasons. The coastal site TF differed from the other two sites with its exceptionally low levels (as low as <50 ppqv) in the nocturnal inversion layer in late summer and early fall and peak levels frequently exceeding 250 ppqv leading to larger diurnal, seasonal, and annual variability. The low values were attributed to nighttime loss via dissolution in dew water in the nocturnal inversion layer and subsequently its re-volatilization in the morning likely comprised the major fraction of the daytime peak level.

Decreasing trends in background Hg^0 were identified in the 7- and 5-yr records at TF and PM with decline rates of 3.3 ppqv yr^{-1} and 6.3 ppqv yr^{-1} , respectively. Year-to-year variability was observed in the warm season decline in Hg^0 at TF varying from a minimum total seasonal loss of 20 ppqv in 2010 to 92 ppqv in 2005, whereas variability remained small at AI and PM. Measurements of Hg^0 at PM, the elevated rural site, exhibited the smallest diurnal to annual variability among the three environments, where peak levels rarely exceeded 250 ppqv and the minimum was typically 100 ppqv. It indicates that there were more complicated processes in the coastal and marine environments causing large temporal variability in Hg^0 .

It should be noted that summertime diurnal variation at TF and AI are opposite in phase indicating strong sink(s) for Hg^0 during the day in the marine boundary layer, which is consistent with the hypothesis of Hg^0 oxidation by halogen radicals there. Moreover, site differences suggest that at elevated inland rural locations interannual variability in ambient levels of Hg^0 is largely driven by processes in summer, while in the coastal and marine environments downwind of major source regions the net effect of all processes can vary greatly from year to year in all seasons but summer.

Mixing ratios of RGM in the coastal and marine boundary layers reached the annual maximum in spring and minimum in fall whereas at the rural elevated location rarely went above the LOD except in spring. RGM levels at AI appeared to be larger than TF and PM in most seasons indicating stronger source strength(s) in the marine environment, and nighttime levels at AI were often above the LOD. Diurnal variation of RGM

Part 1: Temporal variability

H. Mao and R. Talbot

Title Page

Abstract

Introduction

Conclusions

References

Tables

Figures

◀

▶

◀

▶

Back

Close

Full Screen / Esc

Printer-friendly Version

Interactive Discussion



was most pronounced with peaks during the day and minimums at night in spring and summer at TF and AI and at PM in spring only.

Mixing ratios of Hg^{P} at AI and TF were close in magnitude to RGM levels and were mostly below 1 ppqv. Observations at TF revealed that the annual maxima occurred in winter and the minima in fall, which is similar to the annual cycle of RGM. For Hg^{P} diurnal variation was barely discernible at TF and AI in spring and summer with higher levels during the day and smaller but always above LOD at night in nearly all seasons.

Future work is warranted to understand mechanisms driving the site difference and temporal variabilities of Hg^{O} , RGM, and Hg^{P} in the three environments. In our Part 2 (Mao et al., 2011) and 3 (Mao and Talbot, 2011) we will investigate the relationships that Hg^{O} , RGM and Hg^{P} may have with physical variables and other chemical compounds.

Acknowledgements. Funding for this work is provided by the National Science Foundation under grant # ATM1141713, the National Oceanic and Atmospheric Administration AIRMAP program under grant # NA07OAR4600514, and the Environmental Protection Agency under contract # EP09H000355. We thank Cheryl Parker and Kevan Carpenter for technical support. We thank J. Sigler for his work on initiating and maintaining RGM measurement at AIRMAP sites.

References

- Cole, A. S. and Steffen, A.: Trends in long-term gaseous mercury observations in the Arctic and effects of temperature and other atmospheric conditions, *Atmos. Chem. Phys.*, 10, 4661–4672, doi:10.5194/acp-10-4661-2010, 2010.
- Ebinghaus, R., Kock, H. H., Coggins, A. M., Spain, T. G., Jennings, S. G., and Temme, C.: Long-term measurements of atmospheric mercury at Mace Head, Irish west coast, between 1995 and 2001, *Atmos. Environ.*, 36, 5267–5276, 2002.
- Ebinghaus, R., Jennings, S. G., Kock, H. H., Derwent, R. G., Manning, A. J., and Spain, T. G.: Decreasing trend in total gaseous mercury observations in baseline air at Mace Head, Ireland, from 1996 to 2009, *Atmos. Environ.*, 45, 3475–3480, 2011.
- Feddersen, D. M., Talbot, R., and Mao, H.: Size distribution of particulate mercury in marine and continental atmospheres, *Atmosphere*, in preparation, 2011.

Part 1: Temporal variability

H. Mao and R. Talbot

Title Page

Abstract

Introduction

Conclusions

References

Tables

Figures

◀

▶

◀

▶

Back

Close

Full Screen / Esc

Printer-friendly Version

Interactive Discussion



Part 1: Temporal variability

H. Mao and R. Talbot

[Title Page](#)[Abstract](#)[Introduction](#)[Conclusions](#)[References](#)[Tables](#)[Figures](#)[◀](#)[▶](#)[◀](#)[▶](#)[Back](#)[Close](#)[Full Screen / Esc](#)[Printer-friendly Version](#)[Interactive Discussion](#)

- Fu, X., Feng, X., Zhu, W., Zheng, W., Wang, S., and Lu, J. Y.: Total particulate and reactive gaseous mercury in ambient air on the eastern slope of the Mt. Gongga, China, *Appl. Geochem.*, 23, 408–418, 2008.
- Kim, S. Y.: Continental outflow of polluted air from the U.S. to the North Atlantic and mercury cycling in various Atmospheric environments, Ph.D. dissertation, 114 pp., University of New Hampshire, September 2010.
- Landis, M. S., Stevens, R. K., Schaedlich, F., and Prestbo, E. M.: Development and characterization of an annular denuder methodology for the measurement of divalent inorganic reactive gaseous mercury in ambient air, *Environ. Sci. Technol.*, 36, 3000–3009, 2002.
- Laurier, F. J. G., Mason, R. P., and Whalin, L.: Reactive gaseous mercury formation in the North Pacific Ocean's marine boundary layer: A potential role of halogen chemistry, *J. Geophys. Res.*, 108, 4529, doi:10.1029/2003JD003625, 2003.
- Laurier, F. and Mason, R.: Mercury concentration and speciation in the coastal and open ocean boundary layer, *J. Geophys. Res.*, 112, D06302, doi:10.1029/2006JD007320, 2007.
- Lombard, M. A. S., Bryce, J. G., Mao, H., and Talbot, R.: Mercury deposition in Southern New Hampshire, 2006–2009, *Atmos. Chem. Phys.*, 11, 7657–7668, doi:10.5194/acp-11-7657-2011, 2011.
- Mason, R. P. and Sheu, G.-R.: Role of the ocean in the global mercury cycle, *Global Bio. Cycles*, 16, 1093, doi:10.1029/2001GB001440, 2002.
- Mason, R. P., Laurier, F. J. G., Whalin, L., and Sheu, G.-R.: The role of ocean-atmosphere exchange in the global mercury cycle, *J. Phys. IV France*, 107, 835–838, doi:10.1051/jp4:20030428, 2003.
- Mao, H. and Talbot, R.: O₃ and CO in New England: Temporal variations and relationships, *J. Geophys. Res.*, 109, D21304, doi:10.1029/2004JD004913, 2004.
- Mao, H. and Talbot, R.: Long-term variation in speciated mercury at marine, coastal and inland sites in New England – Part 3: Relationships with Atmospheric Chemical Compounds, to be submitted to *Atmos. Chem. Phys. Discuss.*, 2011.
- Mao, H., Talbot, R. W., Sigler, J. M., Sive, B. C., and Hegarty, J. D.: Seasonal and diurnal variations of Hg⁰ over New England, *Atmos. Chem. Phys.*, 8, 1403–1421, doi:10.5194/acp-8-1403-2008, 2008.
- Mao, H., Talbot, R., Hegarty, J., and Koermer, J.: Speciated mercury at marine, coastal, and inland sites in New England – Part 2: Relationships with atmospheric physical parameters, *Atmos. Chem. Phys. Discuss.*, 11, 28395–28443, doi:10.5194/acpd-11-28395-2011, 2011.

Part 1: Temporal variability

H. Mao and R. Talbot

Title Page

Abstract

Introduction

Conclusions

References

Tables

Figures

◀

▶

◀

▶

Back

Close

Full Screen / Esc

Printer-friendly Version

Interactive Discussion



- Pirrone, N., Ferrara, R., Hedgecock, I. M., Kallos, G., Mamane, Y., Munthe, J., Pacyna, J. M., Pytharoulis, I., Sprovieri, F., Voudouri, A., and Wanberg, I.: Dynamic processes of mercury over the Mediterranean region, *Atmos. Environ.*, 37, S21–S39, 2003.
- Schroeder, W. H. and Munthe, J.: Atmospheric mercury – an overview, *Atmos. Environ.*, 5, 809–822, 1998.
- 5 Sheu, G.-R.: Speciation and distribution of atmospheric mercury: Significance of reactive gaseous mercury in the global mercury cycle, Ph.D. Thesis, University of Maryland, College Park, 170 pp., 2001.
- Sigler, J. M. and Lee, X.: Gaseous mercury in background forest soil in the northeastern United States, *J. Geophys. Res.*, 111, G02007, doi:10.1029/2005JG000106, 2006.
- 10 Sigler, J. M., Mao, H., and Talbot, R.: Gaseous elemental and reactive mercury in Southern New Hampshire, *Atmos. Chem. Phys.*, 9, 1929–1942, doi:10.5194/acp-9-1929-2009, 2009.
- Slemr, F., Brunke, E.-G., Ebinghaus, R., and Kuss, J.: Worldwide trend of atmospheric mercury since 1995, *Atmos. Chem. Phys.*, 11, 4779–4787, doi:10.5194/acp-11-4779-2011, 2011.
- 15 Sprovieri, F., Pirrone, N., and Sommar, J.: Mercury speciation in the marine boundary layer along a 6000 km cruise path around the Mediterranean Sea, *Atmos. Environ.*, 37, suppl. 1, S63–S71, 2003.
- Sprovieri, F., Pirrone, N., Ebinghaus, R., Kock, H., and Dommergue, A.: A review of worldwide atmospheric mercury measurements, *Atmos. Chem. Phys.*, 10, 8245–8265, doi:10.5194/acp-10-8245-2010, 2010.
- 20 Talbot, R., Mao, H., Feddersen, D., Smith, M., Kim, S. Y., Sive, B., Haase, K., Ambrose, J., Zhou, Y., and Russo, R.: Comparison of particulate mercury measured with manual and automated methods, *Atmosphere*, 2, 1–20, doi:10.3390/atmos2010001, 2011.
- Valente, R. J., Shea, C., Humes, K. L., and Tanner, R. L.: Atmospheric mercury in the Great Smoky Mountains compared to regional and global levels, *Atmos. Environ.*, 41, 1861–1873, 2007.
- 25 Zhang, L., Wright, L. P., and Blanchard, P.: A review of current knowledge concerning dry deposition, of atmospheric mercury, *Atmos. Environ.*, 43, 5853–5864, 2009.

Table 1. The lower 10th, median and 90th percentile values of Hg⁰ (ppqv) at AI, TF, and PM. The seasonal sample size is given under “N”.

	AI				TF				PM			
	N	10th	Med	90th	N	10th	Med	90th	N	10th	Med	90th
2004 Winter					24 537	154	166	179				
Spring					24 974	140	157	179				
Summer					25 255	114	136	156				
Fall					24 462	114	138	162				
2005 Winter					13 771	153	168	192				
Spring					19 870	149	172	198				
Summer					25 079	103	136	161	20 822	145	163	189
Fall					22 367	85	112	143	25 498	136	151	169
2006 Winter					18 528	142	156	185	23 277	147	161	181
Spring					18 132	136	156	182	22 767	146	158	174
Summer					16 178	109	131	150	20 177	121	140	159
Fall					18 712	89	127	171	18 704	133	148	164
2007 Winter					18 510	163	178	194	17 351	159	171	186
Spring					18 441	153	179	202	18 574	150	169	187
Summer	14 493	113	157	184	18 906	112	146	172	15 304	131	146	170
Fall	3125	92	106	120	17 642	105	142	173	18 965	123	138	158
2008 Winter	–	–	–	–	18 303	153	171	194	18 842	143	161	180
Spring	10 365	119	140	164	18 684	134	152	177	10 189	138	157	172
Summer	13 870	112	148	187	17 024	101	131	160	18 203	134	152	175
Fall	11 926	102	130	164	15 534	93	127	162	24 373	122	136	155
2009 Winter	11 625	128	156	179	5388	160	174	189	20 547	131	145	157
Spring	11 857	133	154	171	15 955	150	169	186	16 130	131	150	172
Summer	11 610	113	138	163	16 665	114	140	170	21 668	125	138	156
Fall	10 522	104	125	149	15 427	95	118	135	17 647	94	127	148
2010 Winter	5341	134	174	185	16 186	135	150	165	10 714	143	156	168
Spring	12 675	157	174	185	16 698	133	150	163	20 861	140	154	167
Summer	15 879	128	144	167	17 336	119	151	172	16 364	125	138	153

Part 1: Temporal variability

H. Mao and R. Talbot

Title Page

Abstract Introduction

Conclusions References

Tables Figures

◀ ▶

◀ ▶

Back Close

Full Screen / Esc

Printer-friendly Version

Interactive Discussion



Part 1: Temporal variability

H. Mao and R. Talbot

Table 2. The total decrease and increase (ppqv) of Hg^0 as well as its decline and increase rates (ppqv day^{-1} ; in parentheses) during the warm (1 April–30 September) and cool (1 October–28 February) seasons, respectively, at AI, TF, and PM.

	AI		TF		PM	
	warm	cool	warm	cool	warm	cool
2004	–	–	44 (–0.2)	54 (0.5)	–	–
2005	–	–	92 (–0.6)	69 (0.5)	36 (–0.2)	19 (0.1)
2006	–	–	62 (–0.4)	56 (0.4)	47 (–0.2)	39 (0.3)
2007	84* (–0.8)	–	62 (–0.4)	53 (0.4)	49 (–0.2)	37 (0.3)
2008	18 (–0.1)	55 (0.3)	48 (–0.3)	52 (0.4)	30 (–0.1)	20 (0.3)
2009	45 (–0.2)	50 (0.3)	43 (–0.3)	52 (0.4)	32 (–0.1)	32* (0.5)
2010	48* (–0.3)	–	11* (–0.1)	–	24* (–0.2)	–

* Denotes the seasons that were shorter due to missing measurement data and shortened study periods and therefore should be used with caution in comparison.

Title Page

Abstract

Introduction

Conclusions

References

Tables

Figures

◀

▶

◀

▶

Back

Close

Full Screen / Esc

Printer-friendly Version

Interactive Discussion



Part 1: Temporal variability

H. Mao and R. Talbot

Table 3. The lower 10th, median and 90th percentile values of RGM (ppqv) at AI, TF, and PM.

	AI				TF				PM			
	<i>N</i>	10th	Med	90th	<i>N</i>	10th	Med	90th	<i>N</i>	10th	Med	90th
2006 11/6-30					276	0.00	0.03	0.34				
2007 Winter					925	0.06	0.24	0.87	635	0.06	0.16	0.54
Spring					865	0.12	0.55	2.48	843	0.02	0.14	0.57
Summer	507	0.18	0.55	1.72	469	0.07	0.26	1.00	586	0.01	0.04	0.19
Fall	143	0.06	0.28	1.03	578	0.07	0.21	0.80	681	0.01	0.04	0.26
2008 Winter	–	–	–	–	671	0.08	0.20	0.59	943	0.01	0.03	0.12
Spring	439	0.07	0.50	1.92	733	0.10	0.35	1.57	347	0.01	0.05	0.22
Summer	635	0.05	0.21	1.16	299	0.00	0.12	0.65	717	0.00	0.02	0.10
Fall	253	0.02	0.13	0.58	302	0.05	0.14	0.59				
2009 Winter	333	0.12	0.36	0.92	220	0.17	0.42	0.97				
Spring	584	0.10	0.37	1.34	652	0.08	0.41	1.52				
Summer	306	0.07	0.21	0.78	594	0.04	0.13	0.43				
Fall	279	0.08	0.29	1.63	428	0.03	0.09	0.30				
2010 Winter	206	0.01	0.03	0.09	401	0.03	0.09	0.37				
Spring	518	0.02	0.14	0.78	514	0.04	0.16	0.94				
Summer	609	0.06	0.23	1.43	537	0.02	0.10	0.70				

[Title Page](#)
[Abstract](#)
[Introduction](#)
[Conclusions](#)
[References](#)
[Tables](#)
[Figures](#)
[◀](#)
[▶](#)
[◀](#)
[▶](#)
[Back](#)
[Close](#)
[Full Screen / Esc](#)
[Printer-friendly Version](#)
[Interactive Discussion](#)


Part 1: Temporal variability

H. Mao and R. Talbot

Table 4. The 10th, 50th, and 90th percentile values (ppqv) of Hg^{P} at TF and AI.

	TF				AI			
	<i>N</i>	10th	Med	90th	<i>N</i>	10th	Med	90th
2009 February	220	0.43	0.88	1.71				
Spring	634	0.12	0.36	1.14	290	0.07	0.19	0.55
Summer	660	0.09	0.25	0.57	489	0.10	0.33	0.73
Fall	461	0.06	0.15	0.41	400	0.09	0.25	1.27
2010 Winter	451	0.08	0.39	0.98	237	0.04	0.09	0.20
Spring	579	0.08	0.26	0.59	566	0.03	0.21	0.81
Summer	694	0.09	0.35	0.77	691	0.16	0.52	0.98

[Title Page](#)
[Abstract](#)
[Introduction](#)
[Conclusions](#)
[References](#)
[Tables](#)
[Figures](#)
[I◀](#)
[▶I](#)
[◀](#)
[▶](#)
[Back](#)
[Close](#)
[Full Screen / Esc](#)
[Printer-friendly Version](#)
[Interactive Discussion](#)


Part 1: Temporal variability

H. Mao and R. Talbot

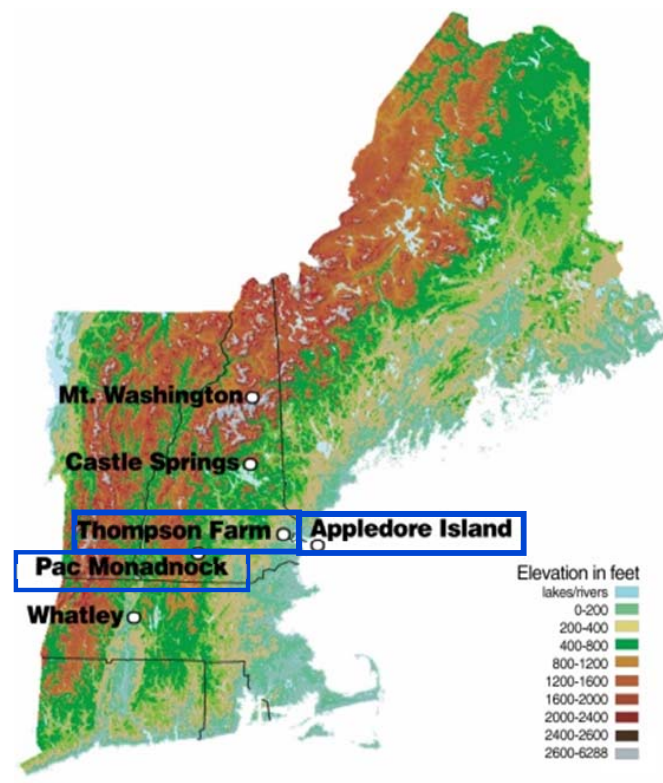


Fig. 1. Locations of the AIRMAP air quality monitoring stations. Thompson Farm, Pac Monadnock, and Appledore Island are highlighted in blue boxes.

Title Page

Abstract	Introduction
Conclusions	References
Tables	Figures

◀
▶

◀
▶

Back	Close
------	-------

Full Screen / Esc

Printer-friendly Version

Interactive Discussion



Part 1: Temporal variability

H. Mao and R. Talbot

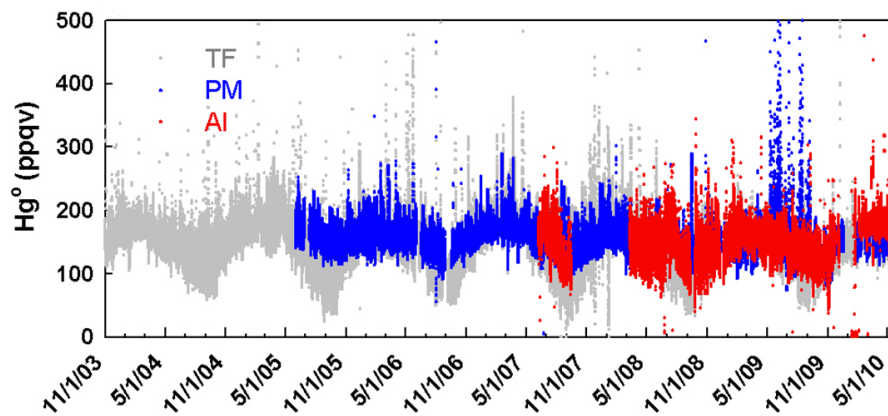


Fig. 2. Complete time series of 5-min average Hg^0 at Thompson Farm (TF) (gray), Pac Monadnock (PM) (blue), and Appledore Island (AI) (red).

[Title Page](#)[Abstract](#)[Introduction](#)[Conclusions](#)[References](#)[Tables](#)[Figures](#)[I◀](#)[▶I](#)[◀](#)[▶](#)[Back](#)[Close](#)[Full Screen / Esc](#)[Printer-friendly Version](#)[Interactive Discussion](#)

Part 1: Temporal variability

H. Mao and R. Talbot

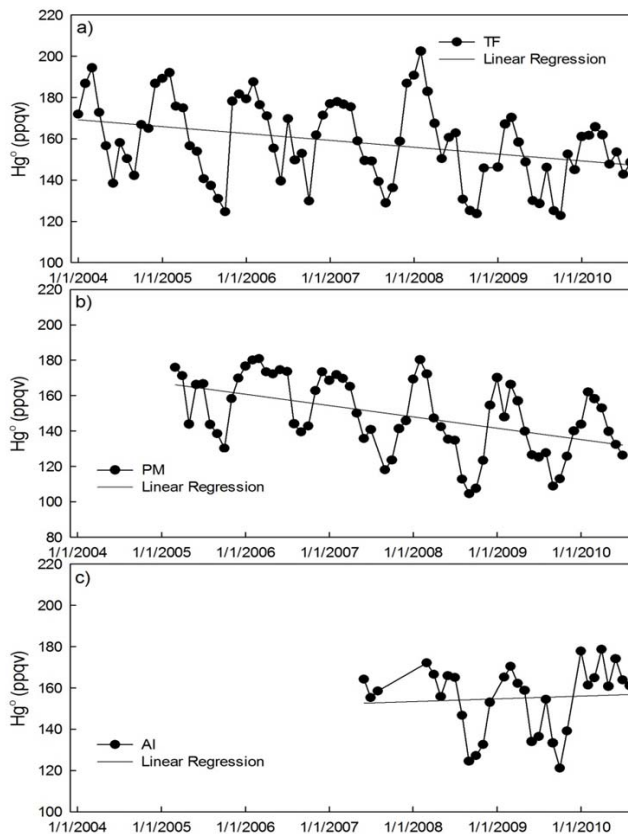


Fig. 3. Monthly median mixing ratios of background Hg^0 at (a) Thompson Farm (TF), (b) Pac Monadnock (PM), and (c) Appledore Island (AI).

Title Page

Abstract Introduction

Conclusions References

Tables Figures

◀ ▶

◀ ▶

Back Close

Full Screen / Esc

Printer-friendly Version

Interactive Discussion



Part 1: Temporal variability

H. Mao and R. Talbot

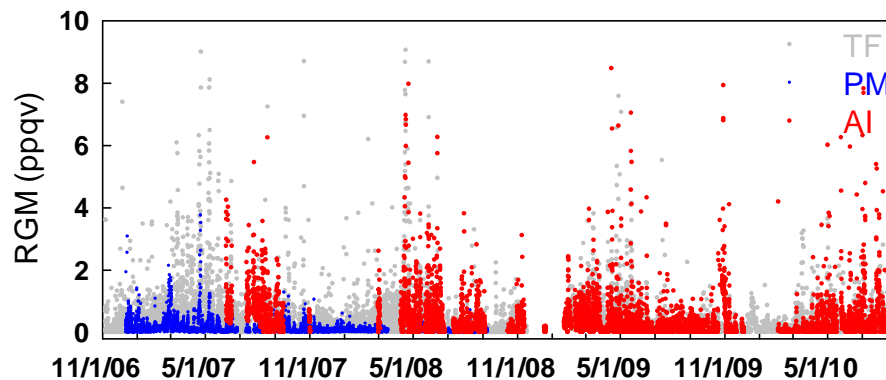


Fig. 4. Complete time series of 2-hourly RGM mixing ratios at Thompson Farm (TF), Pac Monadnock (PM), and Appledore Island (AI).

[Title Page](#)[Abstract](#)[Introduction](#)[Conclusions](#)[References](#)[Tables](#)[Figures](#)[I◀](#)[▶I](#)[◀](#)[▶](#)[Back](#)[Close](#)[Full Screen / Esc](#)[Printer-friendly Version](#)[Interactive Discussion](#)

Part 1: Temporal variability

H. Mao and R. Talbot

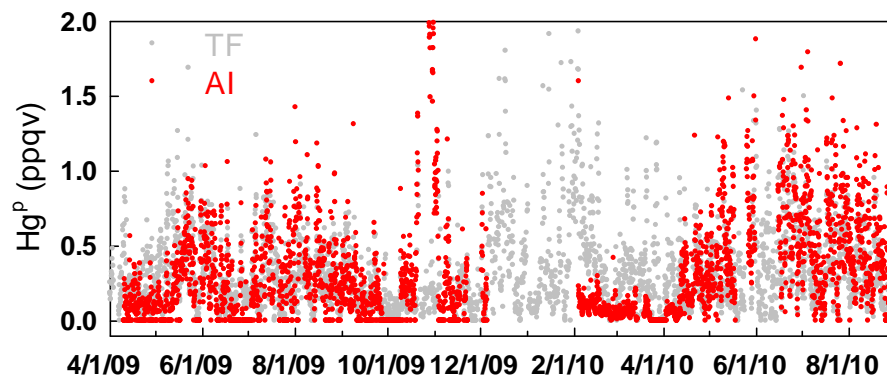


Fig. 5. Complete time series of 2-hourly Hg^{P} at Appledore Island (AI) and Thompson Farm (TF).

[Title Page](#)[Abstract](#)[Introduction](#)[Conclusions](#)[References](#)[Tables](#)[Figures](#)[◀](#)[▶](#)[◀](#)[▶](#)[Back](#)[Close](#)[Full Screen / Esc](#)[Printer-friendly Version](#)[Interactive Discussion](#)

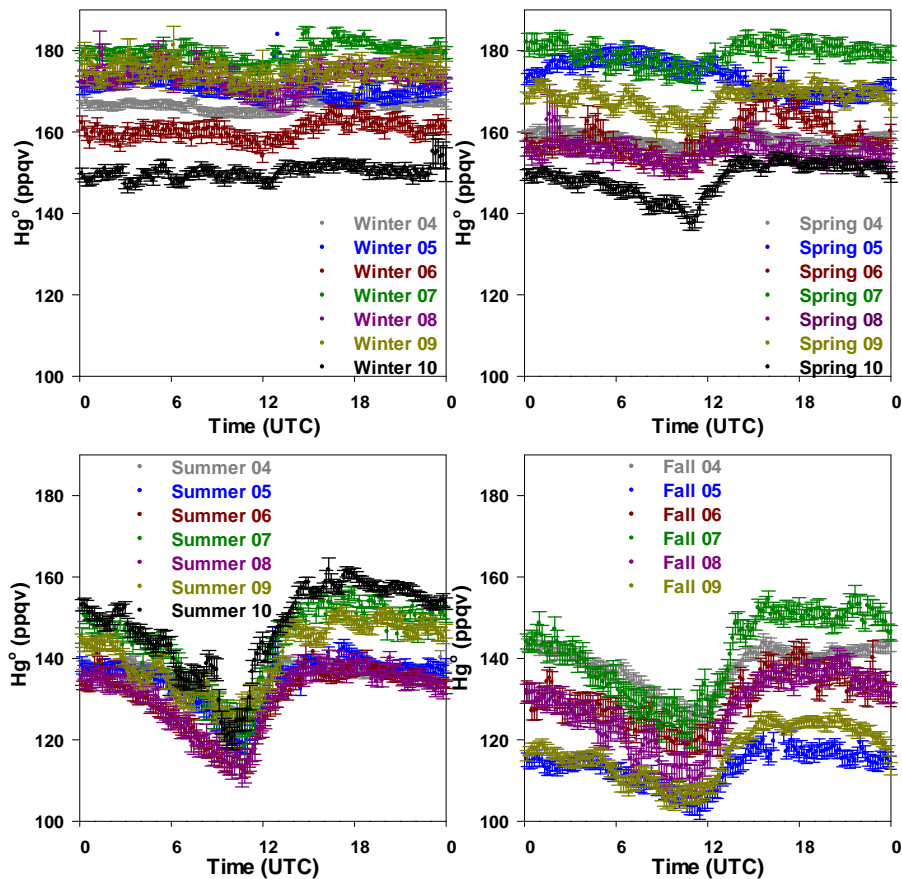


Fig. 6. Seasonally averaged diurnal cycles of Hg^0 with standard deviation of means at TF.

Part 1: Temporal variability

H. Mao and R. Talbot

Title Page

Abstract Introduction

Conclusions References

Tables Figures

◀ ▶

◀ ▶

Back Close

Full Screen / Esc

Printer-friendly Version

Interactive Discussion



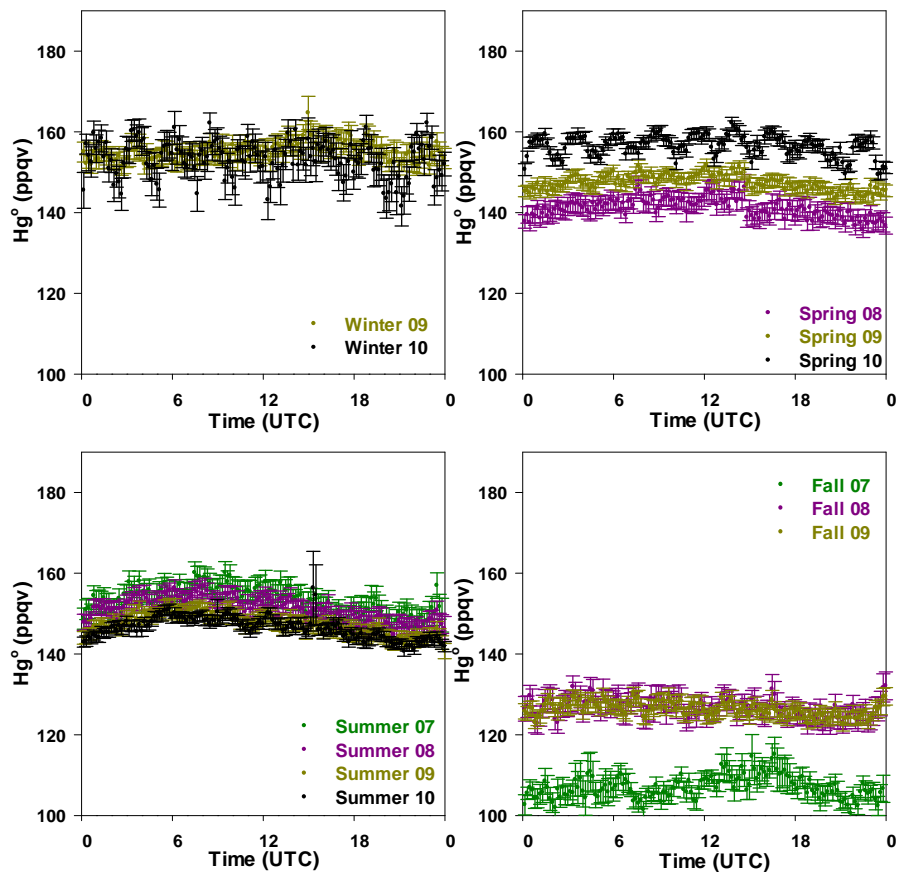


Fig. 7. Seasonally averaged diurnal cycles of Hg° with standard deviation of means at AI. Hg° levels in Fall 07 were nearly 30 ppqv lower than the other two years due to measurement data available only during 1–16 September reflecting the lowest level of Hg° in a year.

Part 1: Temporal variability

H. Mao and R. Talbot

Title Page

Abstract Introduction

Conclusions References

Tables Figures

◀ ▶

◀ ▶

Back Close

Full Screen / Esc

Printer-friendly Version

Interactive Discussion



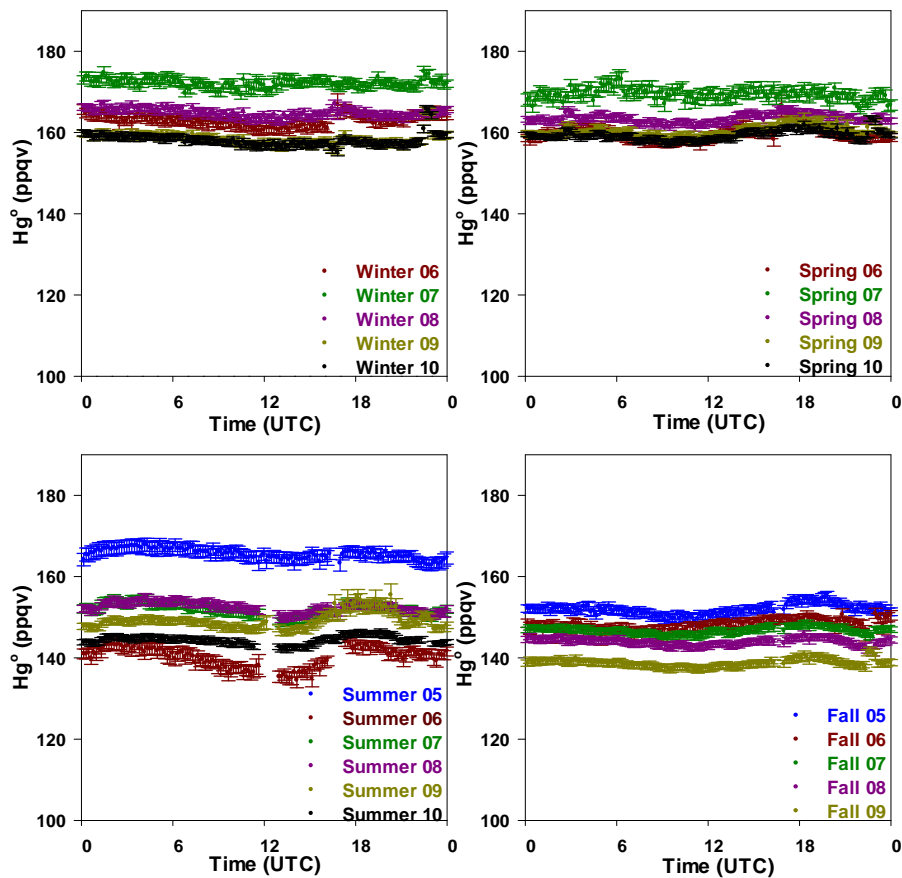


Fig. 8. Seasonally averaged diurnal cycles of Hg^0 with standard deviation of means at PM.

Part 1: Temporal variability

H. Mao and R. Talbot

Title Page

Abstract Introduction

Conclusions References

Tables Figures

◀ ▶

◀ ▶

Back Close

Full Screen / Esc

Printer-friendly Version

Interactive Discussion



Part 1: Temporal variability

H. Mao and R. Talbot

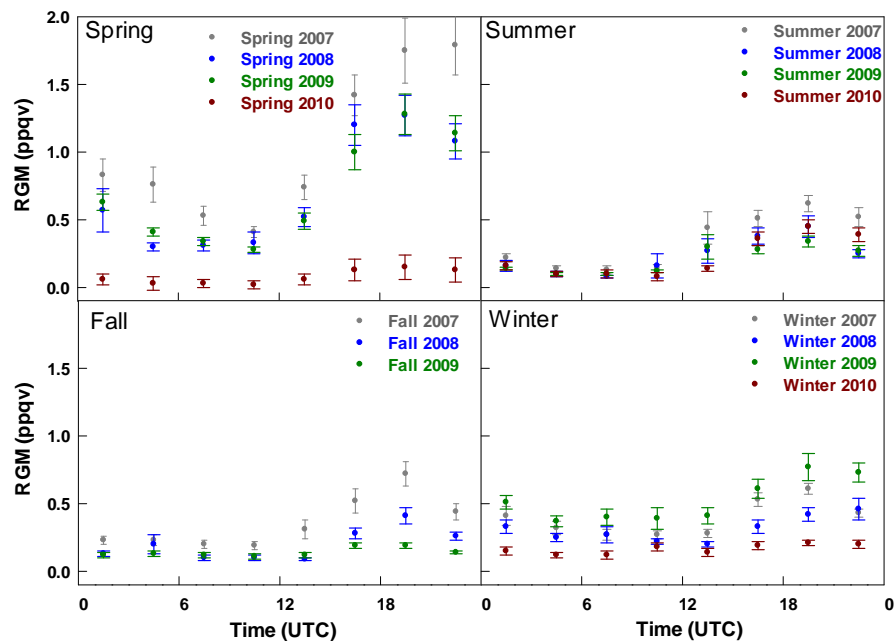


Fig. 9. Seasonally averaged diurnal cycles of RGM with standard deviation of means at TF.

[Title Page](#)[Abstract](#)[Introduction](#)[Conclusions](#)[References](#)[Tables](#)[Figures](#)[◀](#)[▶](#)[◀](#)[▶](#)[Back](#)[Close](#)[Full Screen / Esc](#)[Printer-friendly Version](#)[Interactive Discussion](#)

Part 1: Temporal variability

H. Mao and R. Talbot

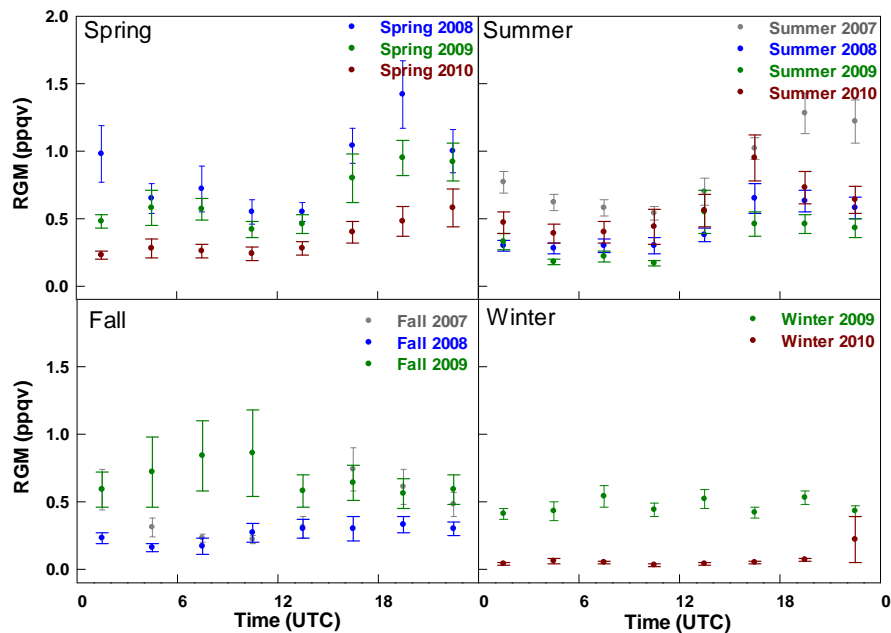
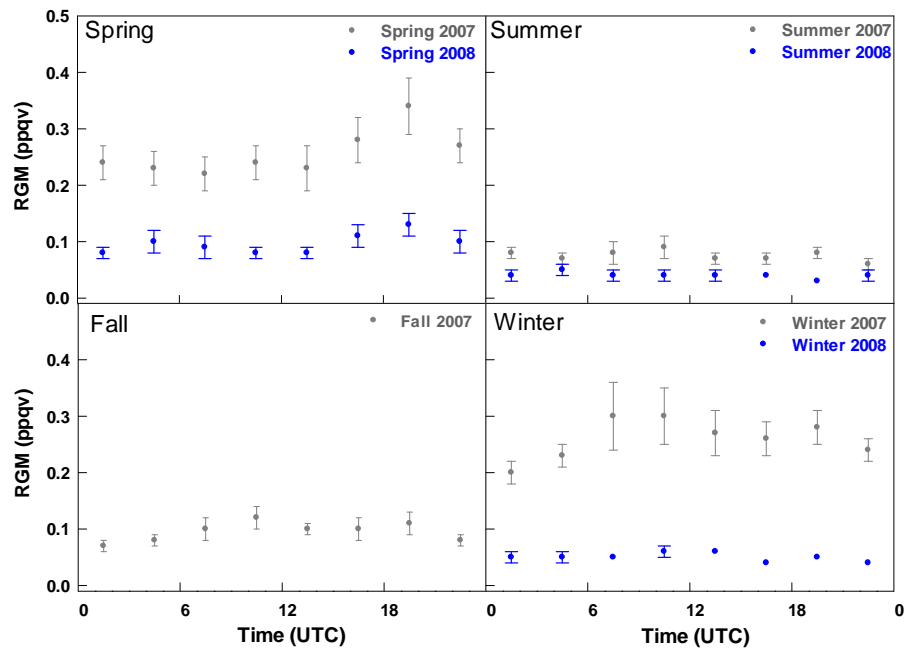


Fig. 10. Seasonally averaged diurnal cycles of RGM with standard deviation of means at AI.

[Title Page](#)[Abstract](#)[Introduction](#)[Conclusions](#)[References](#)[Tables](#)[Figures](#)[◀](#)[▶](#)[◀](#)[▶](#)[Back](#)[Close](#)[Full Screen / Esc](#)[Printer-friendly Version](#)[Interactive Discussion](#)

Part 1: Temporal variability

H. Mao and R. Talbot

**Fig. 11.** Seasonally averaged diurnal cycles of RGM with standard deviation of means at PM.[Title Page](#)[Abstract](#)[Introduction](#)[Conclusions](#)[References](#)[Tables](#)[Figures](#)[◀](#)[▶](#)[◀](#)[▶](#)[Back](#)[Close](#)[Full Screen / Esc](#)[Printer-friendly Version](#)[Interactive Discussion](#)

Part 1: Temporal variability

H. Mao and R. Talbot

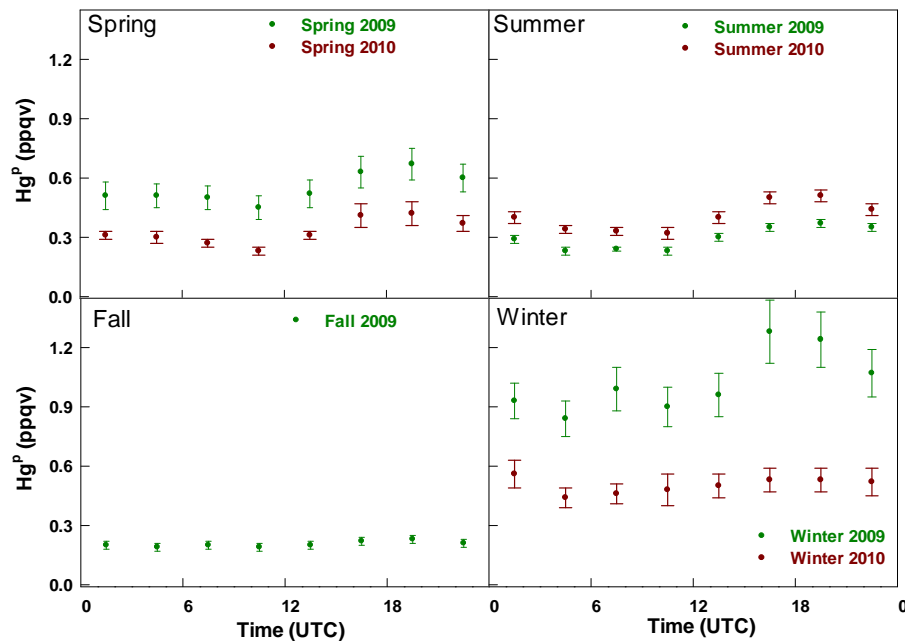


Fig. 12. Seasonally averaged diurnal cycles of Hg^{P} with standard deviation of means at TF.

[Title Page](#)[Abstract](#)[Introduction](#)[Conclusions](#)[References](#)[Tables](#)[Figures](#)[◀](#)[▶](#)[◀](#)[▶](#)[Back](#)[Close](#)[Full Screen / Esc](#)[Printer-friendly Version](#)[Interactive Discussion](#)

Part 1: Temporal variability

H. Mao and R. Talbot

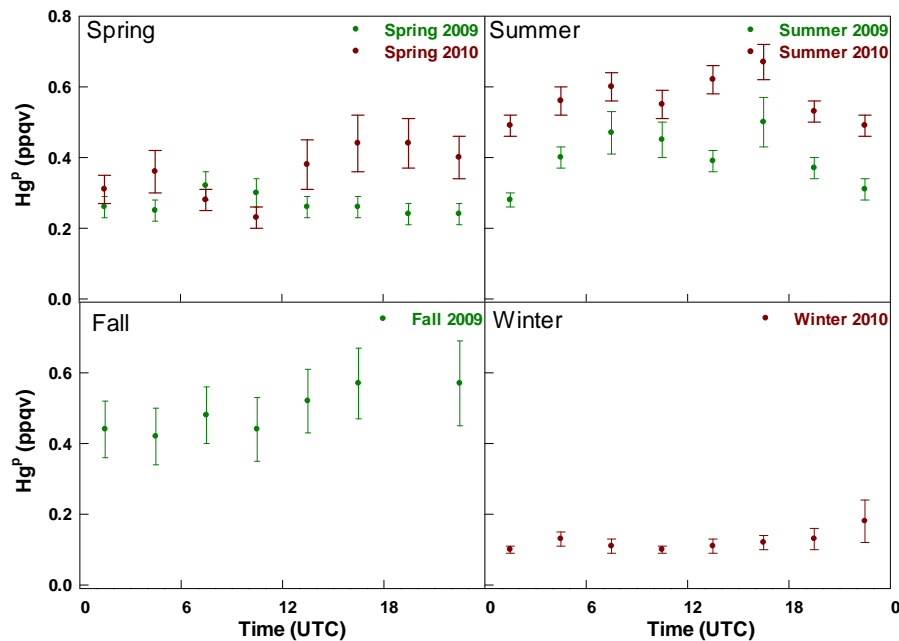


Fig. 13. Seasonally averaged diurnal cycles of Hg^{P} with standard deviation of means AI.

Title Page

Abstract

Introduction

Conclusions

References

Tables

Figures

◀

▶

◀

▶

Back

Close

Full Screen / Esc

Printer-friendly Version

Interactive Discussion

